Influence of thickness and coatings morphology in the antimicrobial performance of zinc oxide coatings.

P. Carvalho[1], P. Sampaio[2], J. O. Carneiro[1], C.Vaz[2], J. P. Espinós[3], V. Teixeira[1]

[1] Department of Physics, University of Minho, Campus de Azurém, 4800-058 Guimaraes, Portugal

[2] CBMA, University of Minho, Campus de Gualtar, 4700 Braga, Portugal

[3] Instituto de Ciencia de Materiales de Sevilla, CSIC-University of Sevilla, Avda. Américo Vespucio 49, 41092 Sevilla, Spain

Abstract

In this research work, the production of undoped and silver (Ag) doped zinc oxide (ZnO) thin films for food packaging applications was developed. The main goal was to determine the influence of coatings morphology and thickness on the antimicrobial performance of the produced samples. The ZnO based thin films were deposited on PET (Polyethylene terephthalate) by means of DC reactive magnetron sputtering. The thin films were characterized by optical spectroscopy, X-Ray Diffraction (XRD), X-ray photoelectron spectroscopy (XPS) and Scanning Electron Microscopy (SEM). The antimicrobial performance of the undoped and Ag-doped ZnO thin films was also evaluated. The results attained have shown that all the deposited zinc oxide and Ag-doped ZnO coatings present columnar morphology with V-shaped columns. The increase of ZnO coatings thickness until 200nm increases the active surface area of the columns. The thinner samples (50 and 100 nm) present a less pronounced antibacterial activity than the thickest ones (200-600nm). Regarding Ag-doped ZnO thin films, it was verified that increasing the silver content decreases the growth rate of *E. coli*. and decreases the amount of bacteria cells present at the end of the experiment.

Keywords: ***ZnO thin films, antimicrobial activity, food packaging***

1. Introduction

More natural, safer and higher quality consumable products have been seen as a market demand of huge importance in what concerns the Food Packaging Industry. Foodborne illnesses and death is rising worldwide, particularly in developed countries[1]. Indeed, data from the Foodborne Diseases Active Surveillance Network (Food Net) states that comparing 2007 with 2004-2006, the estimated occurrence of infections caused by *Campylobacter*, *Listeria*, *Salmonella*, *Shigella*, *Vibrio*, and *Yersinia* did not diminished significantly, and above all, the incidence of *Cryptosporidium* infections even increased by 44% [2]. At the same time, foodborne illness-outbreaks create tremendous social and economic burdens bringing the fear for the re-emergence of infections diseases. Furthermore, the development of antibiotic resistance continues to draw public attention to food safety [3,4]. The combination of the supra-mentioned reasons with the current awareness for environmental conservation and protection has empowered the development of edible coatings and films from biodegradable materials to maintain the quality of both fresh and processed food [5].

Silver-based thin films [6,7,8] and zinc oxide nanoparticles [9,10,11,12,13,14,15] have emerged as promising candidates for active food packaging systems, particularly due to their antibacterial activity. However, due to the lack of knowledge regarding the interactions of nano-sized materials at the molecular and physiological levels and their potential effects on human body, a major concern related to safety of nanoparticles for consumer's health is raising [16,17,18,19]. Titanium dioxide (TiO_2) has been used as a self-cleaning and self-sterilizing material to coat different tools, including sanitary ware, food tableware and cooking ware [20,21]. The antimicrobial effects of TiO_2 are activated by its photocatalytic behaviour, which is totally dependent on ultraviolet and/or visible light irradiation. However, for food packaging industry this is a huge drawback since

the antimicrobial activity will only be effective in irradiated packages. An alternative to overcome this limitation could be the use of Zinc oxide (ZnO). ZnO presents antimicrobial activity, can act as a permeation barrier coating [22] and is Generally Recognized as Safe material (GRAS) by the U.S. Food and Drug Administration (21CFR182.8991). In this sense, the development of zinc oxide thin films can be considered of great added value to food packaging industry. There are a limited amount of scientific publications available describing the interaction between ZnO nanoparticles and bacterial cells and as far the authors knowledge there is no reported work concerning the antimicrobial activity of zinc oxide coatings deposited by means of reactive magnetron sputtering. In this sense, the main goal of this research work is to evaluate the antimicrobial activity of zinc oxide thin films and study the influence of coating thickness, morphology and silver content in the antimicrobial activity. Its applicability for food packaging systems will also be discussed.

To the author's knowledge, this work is the first to study the influence of thickness and coatings morphology on the antimicrobial activity, contributing to the knowledge of important physical variable in the thin films production.

2. Materials and Methods

2.1. Thin films production and characterization

Zinc oxide thin films were deposited on Polyethylene Terephthalate (PET) substrates from Goodfelow and silicon (Si) substrates from Silllicon Materials by reactive DC magnetron sputtering (Advanced Energy Pinnacle Plus, 5K, DC Pulsed). The films deposited on PET were used for the evaluation of the optical properties and the antimicrobial activity and the ones deposited on Si were used for structural, morphological and compositional characterization. It was used a circular zinc target

(Φ=75mm) with a purity of 99,9% and a thickness of 4mm acquired from Goodfellow Before deposition the sputtering chamber was pumped down to 10^{-3} Pa. A gas atmosphere composed by argon (Ar, working gas) and oxygen (O_2, reactive gas) was used in the deposition processes. The Ar and O_2 flows were kept constant at 70 sccm (standard cubic centimetre per minute) and 18 sccm, respectively. Each deposition was carried out with a working pressure of 0.6 Pa, a current of 0.35 A and a target/substrate distance of 80 mm. Prior to each deposition the zinc target was pre-sputtered during 5 minutes. All other deposition parameters were kept constant and the depositions were performed at room temperature (40 ºC measured inside the chamber).

X-ray diffraction (Philips PW 1710 X-ray diffractometer) analysis was used to investigate the crystallographic structure of ZnO thin films. The thickness and morphology of ZnO thin films were obtained by the observation of the cross section of the fractured thin films by SEM (NanoSEM-FEINOVA 200). The optical transmittance was measured by visible spectroscopy (Shimadzu UV-310PC scanning spectrophotometer). The chemical characterization was by using a XPS spectrometer (12 kV, 20 mA) from VG (ESCALAB 210). An unmonocromatized Mg Kα (1253.6 eV) source was used during the measurements. For all the zinc oxide coatings, the binding energies of the XPS spectra were calibrated by using of Zn $2p_{3/2}$ at 1022.2 eV and the spectra were acquired at room temperature. All the coatings were sputtering cleaned with Ar^+ until a stationary composition was achieved. At this stage, no carbon resulting from superficial contamination was observed.

2.2. Thin films antimicrobial activity

In this research work, the *Escherichia coli* was the bacteria species chosen and it was obtained from the Centre of Molecular and Environmental Biology (CBMA), Department of Biology, University of Minho. A pre-culture was prepared for each individual batch experiment. One colony of *E. coli* strain HB101 was picked and loop inoculated into a 125-ml Erlenmeyer flask, containing 20 ml of Luria Bertani (LB) broth (10 g/L tryptone, 10 g/L NaCl, and 5 g/L yeast extract). This pre-culture was incubated at 37°C, for 12 to 15h. On the day after, cells were transferred into different 250-ml Erlenmeyer flasks containing 50 ml of LB broth medium at a starting optical density (OD) of 0.1 measured at a wavelength of 640 nm. A coated PET circular sample (diameter of 6 cm), previously sterilized with 70% ethanol for 1 hour and rinsed in sterile water, was deposited on the bottom of the flask. Flasks were then shaken at 80 rpm in a temperature-controlled incubator at 37 °C, and the OD was monitored every hour. OD measurements were made using a Spectronic 20 instrument at 640 nm and the background (turbidity due to growth medium) was eliminated by taking blank readings. The specific growth rate (μ) was calculated from the exponential phase, according to the following equation:

$$\mu = \frac{1}{t_2 - t_1} \cdot \ln\left(\frac{OD_2}{OD_1}\right) \quad (1)$$

where OD_1 and OD_2 are the optical densities corresponding to time instants t_1 and t_2, respectively. The generation time (t_g) can be calculated according to the equation:

$$t_g = \frac{\ln 2}{\mu} \quad (2)$$

3. Results and discussion

3.1. Thin films structure and morphology

The produced ZnO thin films in this research work are highly transparent, presenting a transmittance of about 80% in the visible region of the electromagnetic spectrum. The remainder 20%, is lost by reflection at the air/ZnO interface, by dispersion and by absorption of light in the substrate.

In order to study the influence of the coating thickness and morphology in its antimicrobial activity, the thickness was controlled by changing the deposition time. With this methodology it was observed that the film thicknesses ranged from 50 to 600 nm. X-ray diffraction analyses were performed in representative samples and the measurements were done between 20º and 70º (2θ) for all thin films. Fig. 1 shows the undoped zinc oxide X-Ray Diffraction patterns of the thin films having 50, 200 and 600 nm thicknesses.

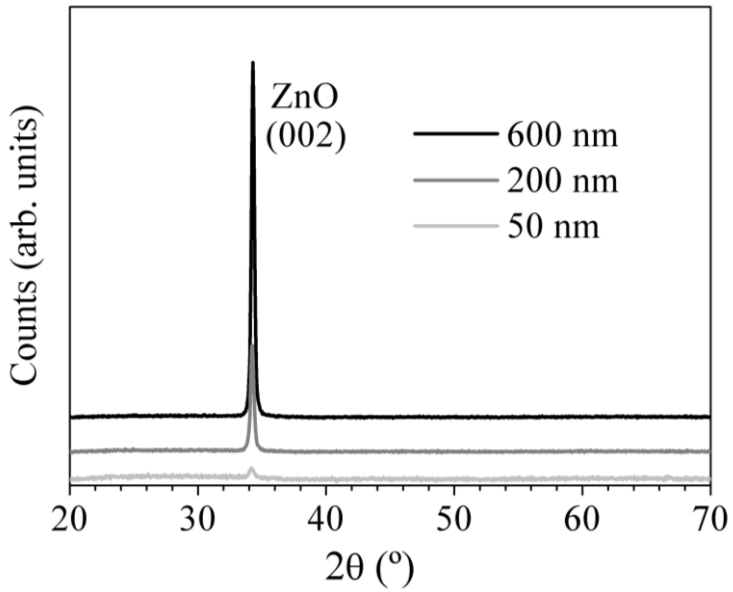

Fig. 1 XRD patterns of ZnO thin films with 50, 200 and 600 nm thickness, deposited in PET substrate.

In XRD patterns it is observed the presence of the (002) diffraction peak of the ZnO wurtzite structure (JPCDS36-1451[23]) in all the samples, indicating a preferential orientation to the c-axis perpendicular to the substrate, as previously reported by others authors[24,25,26]. Some authors correlate the preferential orientation with the minimization of internal stress and surface energy [27,28,29] and others [30] reported that c-orientation maybe result from the highest atomic density found along (002) plane. In Figure 1 it is also possible to observe that, as expected, the increase of the coatings thickness induces an increase of diffraction peak intensity. The decrease of full width at half maximum also suggests an increase of grain size with the thickness.

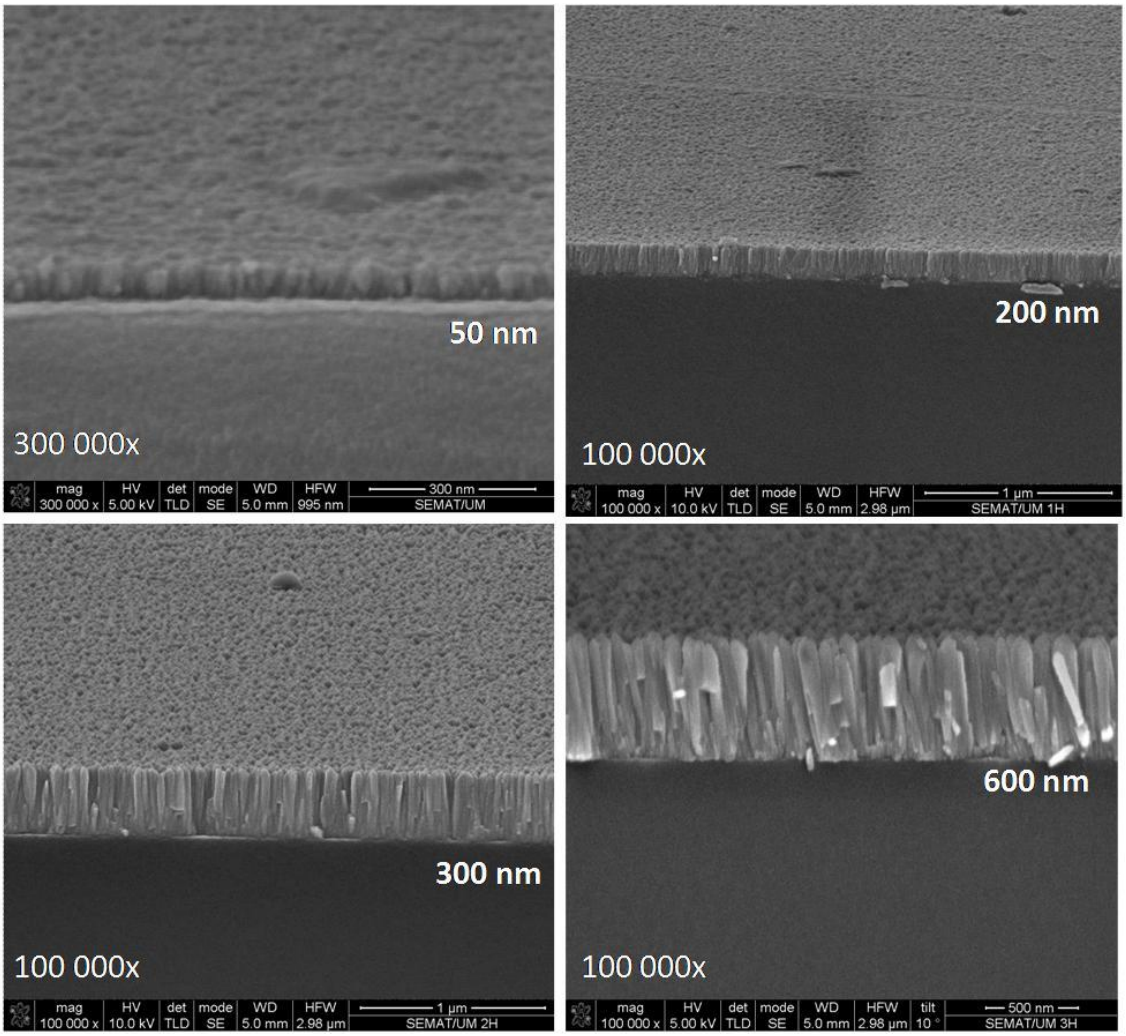

Fig**. 2** shows the SEM micrographs of the undoped ZnO samples cross-sections; the grains extend from the substrate to the top of the film. The typical morphology can

be identified as a Zone 1 film of the modified structure zone model [31] with typically low compactness.

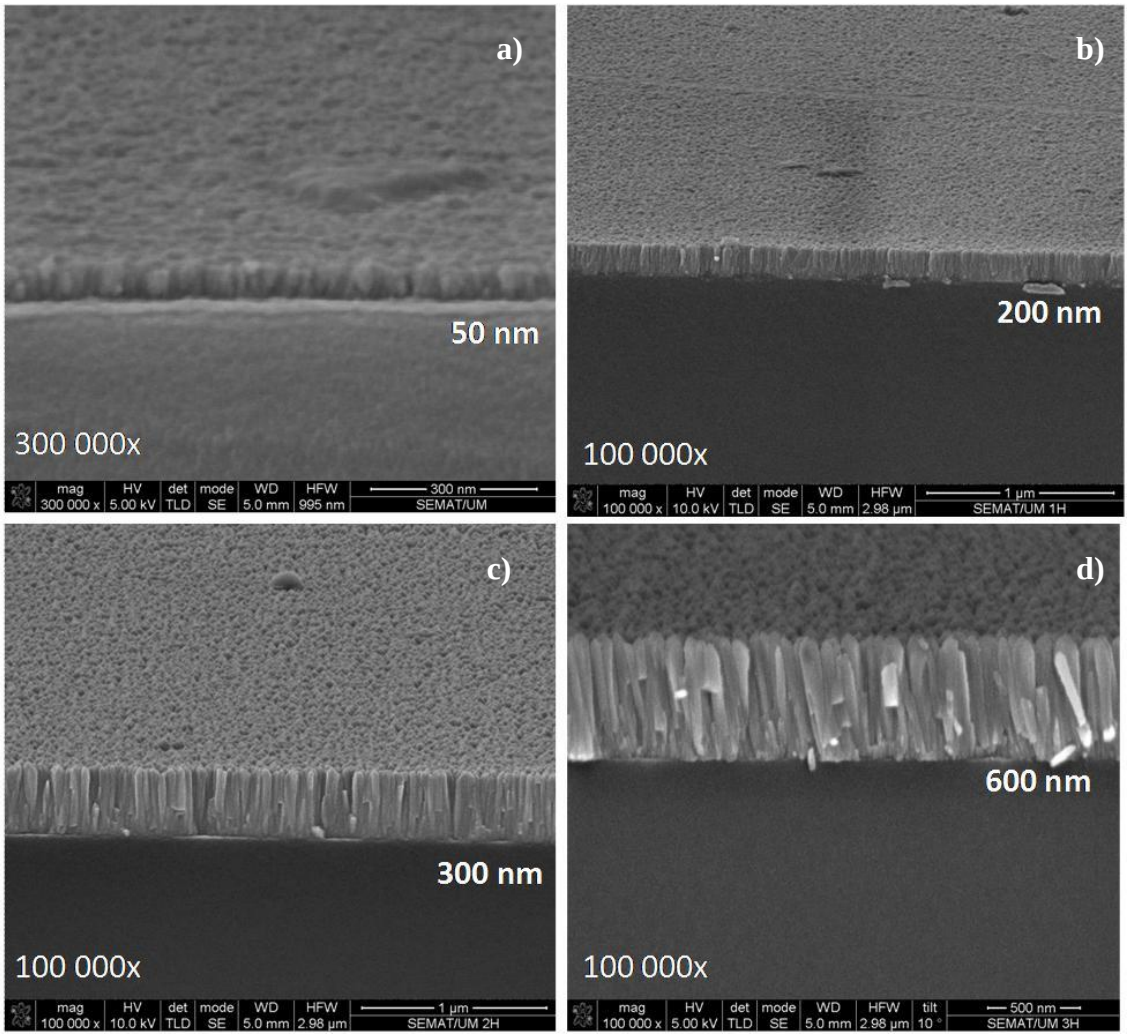

Fig. 2. SEM micrographs presenting the thin films cross-sections with different thickness deposited in Si substrate: a) 50nm; b)200nm; c) 300nm and d) 600nm.

The thinner coatings, 50 and 100 nm (not showed here) present a more compact morphology in comparison with the thickest ones. It is possible to observe that the increase of coatings thickness induces the formation of less compact coatings, with well define and separated columns (**Fig. 2**). From this figure it is can also be identified an increase of columns width with the increase of coatings thickness. From the presented

results it is also possible to conclude that a facet plane can be observed in the upper region for the thickest coatings (300-600 nm). The attained results are in agreement with the ones reported by *J. W. Shin et al.* [32] that deposited ZnO coatings at room temperature on Si substrates. These authors explained the formation of facet planes as being a consequence of the lower diffusion rate of the atoms on the ZnO surface during column's growth the deposition rate.

To better understand the morphology of these coatings, top view SEM micrographs of ZnO samples with different thickness were taken and are shown in Fig. **3**.

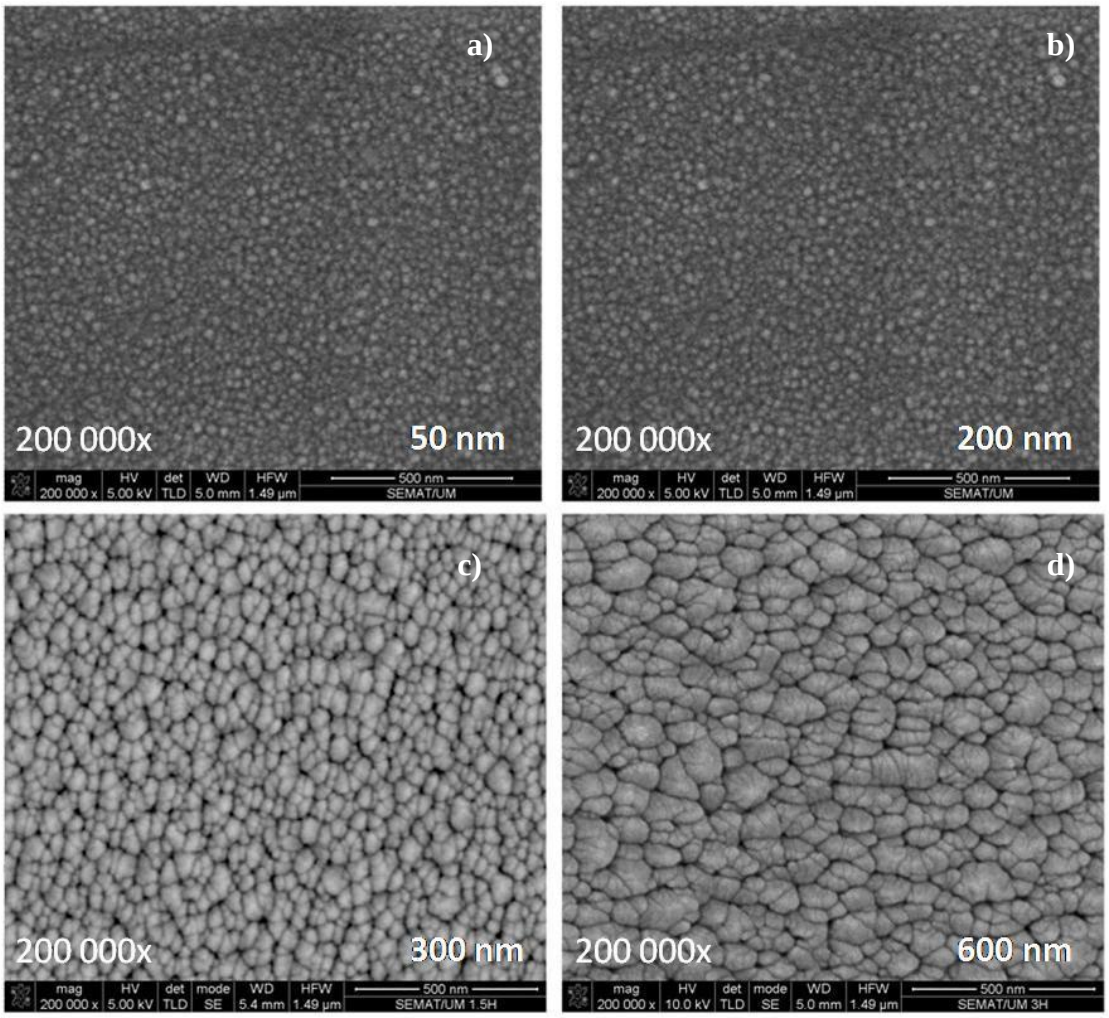

Fig. 3. Top-view SEM micrographs of ZnO thin films with different thickness deposited in Si substrate: a) 50nm; b)200nm; c) 300nm and d) 600nm.

From the last figure it is possible to perceive an increase of the top column width with the increase of the coating's thickness. Since the displayed images (see **Fig. 3**) represent different ZnO coating's growth stages, it is plausible to assume that the deposited zinc oxide coatings have columnar morphology with V-shaped columns.

The formation mechanism of the V-shaped columnar structure has been thoroughly discussed and it is attributed to the competitive growth due to differences in surface energy of neighbouring crystal faces on the free surface of thin films[33,34,35]. A schematic illustration of the ZnO morphology with the increasing thickness is presented in Fig.4.

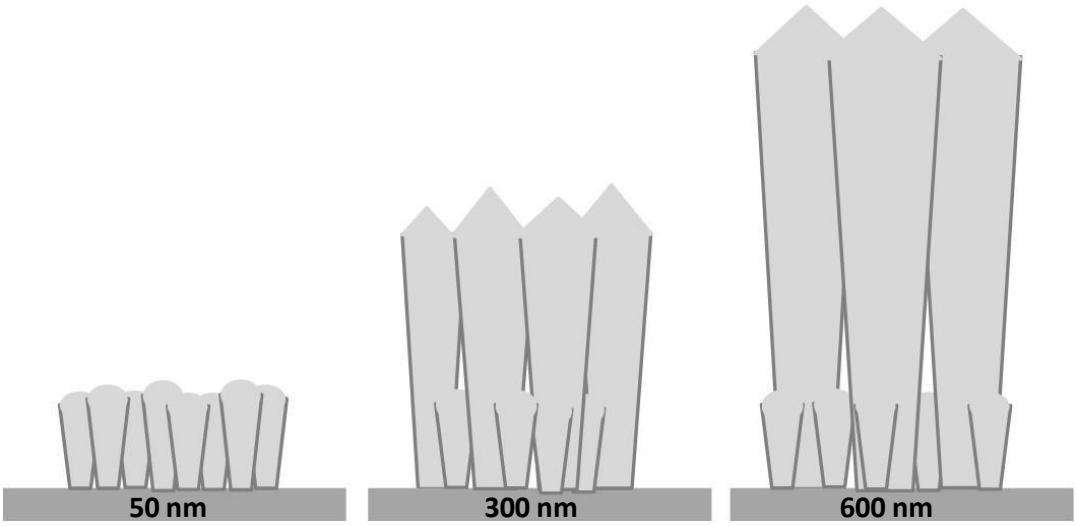

Fig. 4. Scheme of ZnO morphology with increasing thickness.

From the last schema it can be assumed that increasing the thin film's thickness beyond a certain value (that for these specific ZnO films is close to 300 nm) may induce a decrease on the ratio of the columns surface area to columns length.

3.3. Thin film antimicrobial activity

The inhibition effect of the undoped zinc oxide coatings with different thicknesses on the growth rate of *E. coli* was evaluated by incubating bacteria cells with the different coatings in liquid media at very low rotations to enhance the cell contact. Since the optical density (OD) is proportional to the number of microorganisms in the culture medium[36], lower OD indicates a higher antibacterial effect of the coated thin films. The bacterial growth was monitored over more than 24 hours being possible to observe the cultures reaching the stationary phase, in which the microorganisms are no longer able to grow (**Fig. 5A**).

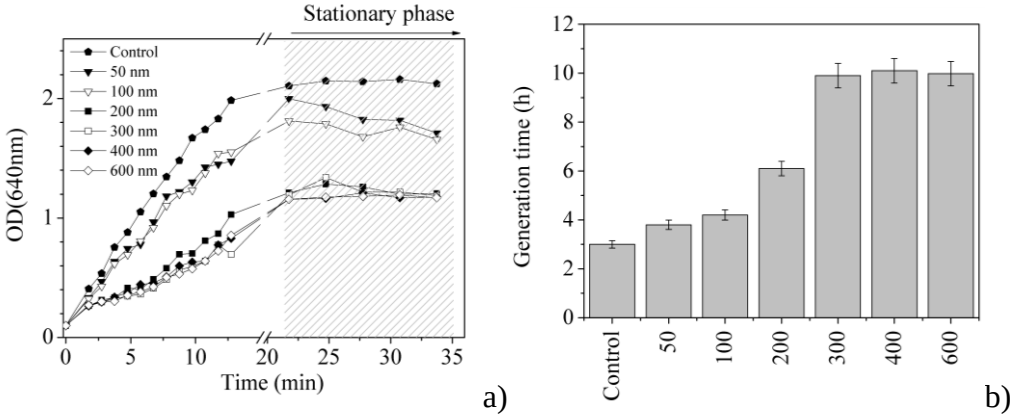

Fig. 5. Antibacterial activities of the ZnO thin films against *E. coli*. A- Bacteria cells were incubated with thin films with different thickness and growth monitored over time measuring OD at 640nm. The control growth was assessed using non coated PET with the same area. B- Generation time of bacteria with thin film thickness.

In fact, Fig. 5 shows that when comparing with the control, the thinner samples (50 and 100 nm) present a less pronounced antibacterial activity than the thickest ones (200-600nm). It is important to point out that the thickest coating (200-600nm) not only increase the generation time, i.e. decrease of the growth rate, (**Fig. 5B**), but also decreased in 45% the amount of bacteria cells present at the end of the experiment. This characteristic is important for food packaging applications since it clearly reduces bacterial load.

The thin films having thicknesses of 50 to 100 nm present an increase of generation time by a factor of 1.26 and 1.4, respectively. By another hand, the thin films with 200 to 600nm induced an increase by a factor from 2 to 3.3, in comparison with the control (Fig. 5b). It can also be observed that samples with thicknesses higher than 200 nm present approximately the same antibacterial activity (Fig. 5b). These results suggest that there exists a maximum thickness above which bacteria growth rate is not further reduced with increasing thickness. In summary, it is possible to conclude that films with 200 to 600 nm were the ones with the best performance in what concerns the reduction of bacteria's growth rate and the total number of bacterial cells.

ZnO powder has been used for a long time as an active antibacterial ingredient for dermatological applications such as creams, lotions and ointments [[37]]. However, ZnO nanoparticles are much more effective agents in controlling the growth of different microorganisms than micro-powders. Some authors [[38],[39],[40],[41]] have been reporting that the smaller the particle size, the greater the efficiency in inhibiting bacteria growth. Moreover, several works showed that the antimicrobial activity is also dependent of the concentration used [[42],[43],[44],[45]]. The higher the concentration of ZnO nano/micro particles, the higher the antibacterial effect achieved. These results indicate that increasing the active surface area enhances the antimicrobial activity. This conclusion could explain the initial increase of the antibacterial performance of the zinc oxide coatings observed in our study from coatings with 50-100 nm to 200-600nm (**Fig. 5**). The contact of moisture in the medium, per unit ZnO mass, increases with the increase of columns length or coating thickness and with the decrease of coatings density. This initial increase in growth inhibition should result from the increase of the surface area resulting from the increase in columns length (coatings thickness). However, this inhibition effect stabilizes at 200nm. The posterior stabilization should result from the

approximately constant surface area. The active surface area depends on three factors, column length, column width and the percentage of voids between columns that are accessible to the species in the liquid phase. As already discussed in this work, associated with the coatings thickness (columns height) enhancement is an increase in the coatings columns width. The increase of columns width can decrease the percentage of voids between columns that are accessible to the species in the liquid phase, keeping constant the active surface area, i.e. the surface area that is accessible to the species in the liquid phase. The satutarion of the active surface area explains the maintenance of the antibacterial performance after stabilization.

After determining the critical thickness of the ZnO coatings on the antibacterial activity of the films, the influence of the silver dopant content in the final properties of the coatings was also evaluated. For this purpose, a new set of samples was deposited, using a constant thickness of ~200nm, but having different Ag/Zn ratio. The Ag/Zn ratio was increased until the average transmittance value in the visible region ($T_{vis.}$) of the coatings decreased to about 80%. Assuming the mentioned restriction ($T_{vis.}$>80%), three different coatings were obtained. The composition data obtained by X-Ray Photoelectron Spectroscopy (XPS) analysis show that the Ag/Zn atomic ratios of the coatings were respectively 0.005(ZnO(Ag)-1), 0.007(ZnO(Ag)-2), and 0.04(ZnO(Ag)-3).

Fig**. 6** shows the XRD patterns of undoped and Ag doped ZnO thin films having different Ag/Zn atomic ratios.

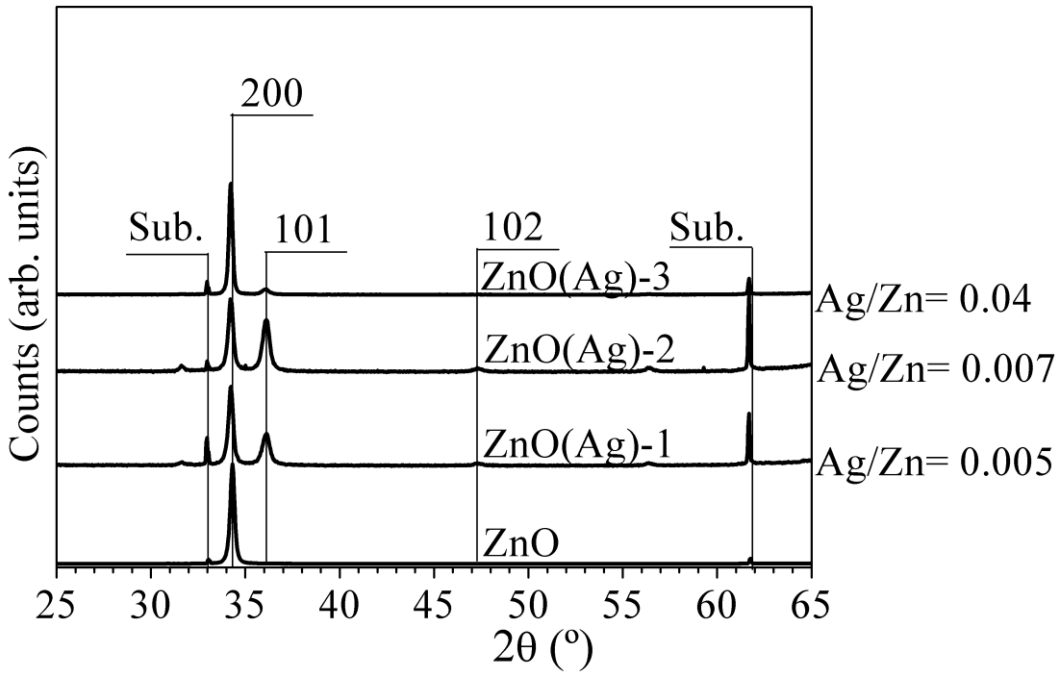

Fig. 6. XRD patterns of silver doped ZnO thin films. It is also included a non doped ZnO sample. All coatings were deposited on Si substrate.

From the diffraction pattern of the last figure it can be observed that the only polycrystalline crystalline phase detected corresponds to the ZnO hexagonal wurtzite type (JPCDS36-1451, a = 0.326 nm and c = 0.522 nm). No phases corresponding to silver or silver oxide were detected, which indicates that there is no additional phase present in the ZnO:Ag films (at least within the limit of X-ray detection). The undoped ZnO sample deposited on Si substrate present similar preferential growth regarding the one deposited on PET substrate, see fig.1. The samples ZnO(Ag)-1 and ZnO(Ag)-2 present several major peaks of ZnO, indicating low extend of crystalline preferential growth. This could indicate that the presence of silver, in very low concentration, may inhibit the c-axis preferential growth of ZnO films. As for the change of c-orientation with Ag doping, some authors [46,47] detected a decrease in the extent of c-orientation while others [48] observed an opposite behaviour by Ag doping. *Oleg Lupa et al.[49]*

proposed that heterogeneous nucleation could be facilitated in the presence of Ag^{+} ions in the ZnO structure, enhancing the growth rate in the (101) direction.

The sample with the highest concentration of silver, ZnO(Ag)-3, present similar XRD spectrum as the undoped ZnO samples, showing a clear c-orientation.

All the Ag doped ZnO films present a small X-Ray Diffraction peak shift as compared with pure ZnO, resulting from the ZnO lattice parameter increased in the c-axis with Ag doping. According to literature [50, 51, 52, 53, 54] the slight decrease of 2θ may be due to the increase of its lattice constant caused by substitution of Zn^{2+} ions (radius of 0.65A˚) by Ag^{+} ions (radius of 1.02A˚) leading to the compressive distortion of the crystalline structure. Due to its large ionic radius, Ag+ would preferentially choose to sit in the vicinity of grain boundaries[55]. Based on first-principles calculations, several authors [56,57] indicated the formation energy for Ag-Zn (Ag in substitutional sites) is lower than that for Ag-i (Ag in interstitial sites). Based on that, if Ag+ ions are available during deposition, it is expected that they may be inserted into ZnO crystalline structure by substitution of Zn^{2+} ions, within the solubility limits. *Shu-Ting Kuo et al*[58] proposed that the solubility of Ag in ZnO is between 0.08 and 0.76 mol%. The same authors, based on the TEM observations, concluded that for higher concentrations above the Ag solubility limit it tend to segregate at the grain boundaries of ZnO. This small value determined by *Shu-Ting Kuo et al*[59] is somehow expected since the large size difference between Zn^{2+} and Ag^{+} ions should reduce the solubility of Ag in ZnO lattice.

Fig. 7 shows the XPS Zn2p and Ag3d spectra of the silver doped and undoped ZnO films.

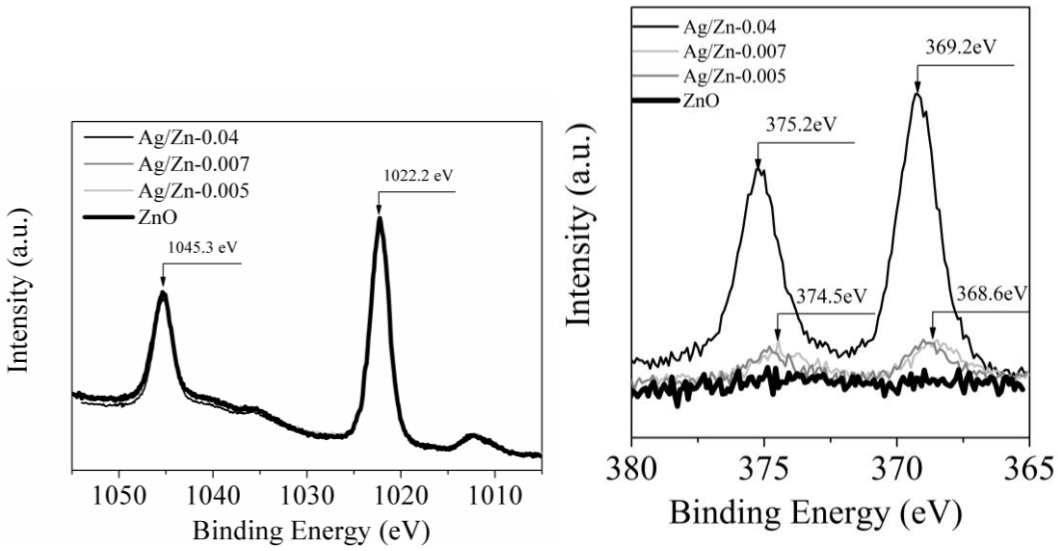

Fig. 7. XPS Zn2p (left) and Ag3d (right) spectra of silver doped ZnO films and undoped ZnO. All coatings were deposited on Si substrate.

The Zn2p3/2 core line, (calibrated at 1022.2 eV[60] of binding energy) exhibits a small asymmetry in the right side, indicating that zinc could present more than one oxidation state. The XPS spectra of Ag3d3/2 peak (**Fig. 7**) shows binding energies in the range 368.6-369.2eV for the three doped samples. The evolution of the binding energy of Ag3d3/2 with the chemical state of silver is anomalous, since it decreases with the oxidation state of this element. The reported silver compound with the highest binding energy is $AlAg_2$ (368.7 eV), and the one with the lowest is AgF_2 (367.7 eV). Binding energies for pure Ag, Ag_2O, and AgO bulk samples are 368.22, 367.8, and 367.4 eV, respectively[61,62,63,64,65,66,67,68]. It is evident that the peak $Ag3d_{5/2}$ in Ag doped ZnO samples are located at energies far above bulk metallic silver (+1 eV) and even above that for bulk $AlAg_2$ (+0.5 eV). Unfortunately, since the surface concentration of silver in doped films is very low, it is not possible to detect properly in these samples the AgMVV Auger signals and, consequently, the value of the modified Auger parameter

of silver, which is so useful to determine the chemical state of this element, cannot be obtained.

We can imagine two different hypothesis that could explain the high binding energy values obtained for $Ag3d_{3/2}$ peaks in ZnO(Ag) films. One, that silver is forming small metal clusters strongly interacting with ZnO support, since it has been widely discussed in the literature that the binding energy of small metallic particles is usually shifted to lower binding energy [69]. For instance, a shift of 0.4 eV was observed for silver deposited on graphite[70], shifts of +0.6 eV [71] and +0.9 eV [72] have been reported for silver on Al_2O_3, while shifts of +0.6 and +1.2 eV have been reported for silver deposited on TiO_2 at 300K and 100K, respectively [73]. These shifts have been attributed to both initial and final state factors affecting the photoemission process. Initial state effects are those affecting the energy of the initial state, as for instance, the metal-substrate interaction, the mean coordination of the atoms in the clusters and their geometry [74,75]. Final state effects are those affecting the relaxation or screening of the photohole, as the Coulombic potential or the dielectric constant of the substrates [76,77]. The binding energy shift observed in our samples, up to +1.0 eV, would be in the upper limit of the range found for small silver clusters on Al_2O_3 and TiO_2. To verify the validity of this hypothesis, we have carried out an experiment in our laboratory where increasing amounts of pure silver are condensed under ultra high vacuum on ZnO films, from a fraction of a monolayer to many monolayers. Note that, regardless of the growth mechanism followed by silver depositing on ZnO (layer by layer or three dimensional island growth), the mean particle size will increases when the deposited amount increases. The result of this experiment is illustrated in **Fig. 8**, where the evolution of Ag3d spectrum is displayed as a function of the nominal thickness of deposited silver, and in **Fig.** 9, where the evolution of the $Ag3d_{5/2}$ peak binding energy is plot versus the

same variable. As can be seen, when deposited on ZnO, the binding energy of very small silver aggregates only shift up to +0.6 eV in respect to that one of bulk silver, which is quite lower than the experimental binding energy value found for Ag doped ZnO films.

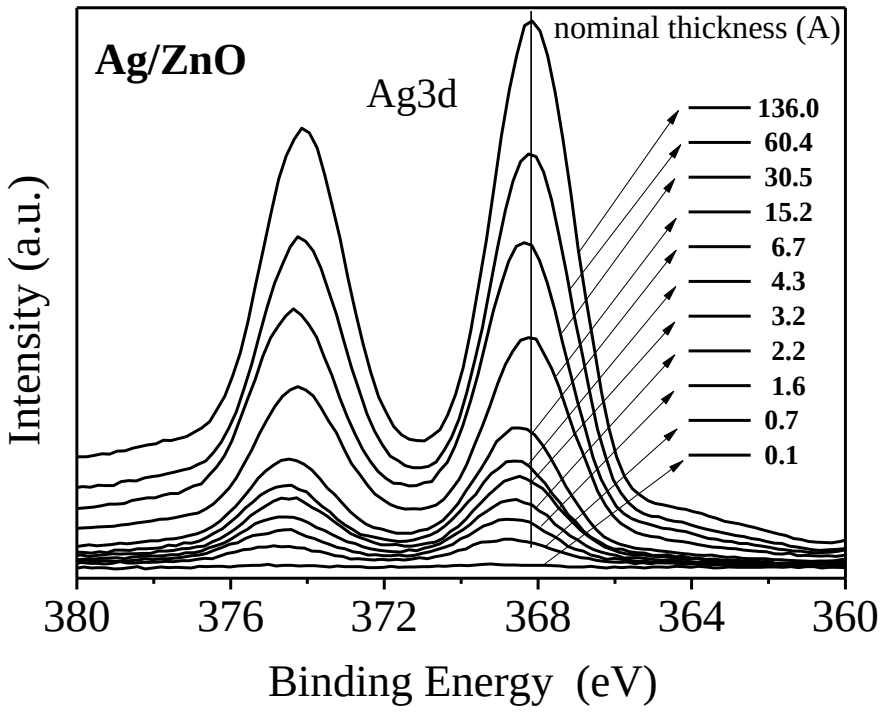

Fig. 8. Evolution of Ag3d spectrum for growing amounts of metal silver deposited under UHV on ZnO. The nominal thickness of deposited silver, assuming a layer to layer growth mode, is expressed in Angstroms.

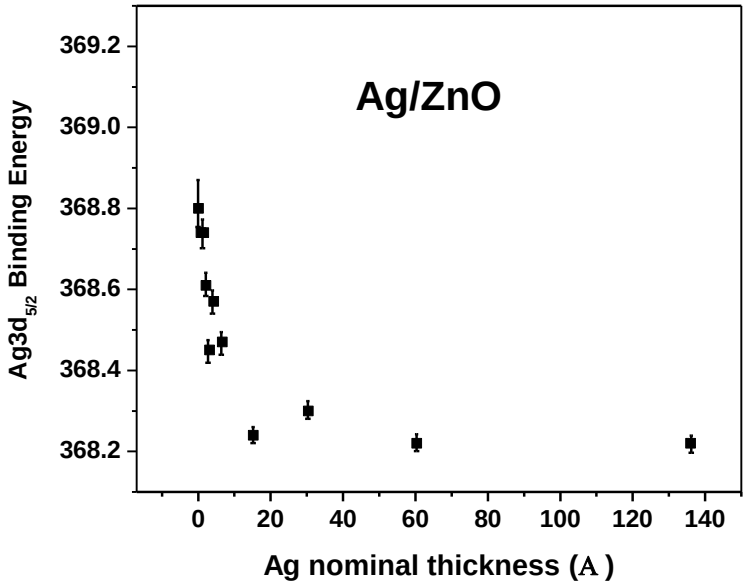

Fig. 9. Evolution of the $Ag3d_{5/2}$ binding energy of silver for deposits of silver on ZnO with growing nominal thickness.

A second possible hypothesis to explain the high binding energy found for silver in Ag/ZnO, is that metal Ag particles are doped with metal Zn, giving rise to the formation of an intermetallic compound, where the binding energy of $Ag3d_{3/2}$ signal could be higher than that for pure silver, as reported for $AlAg_2$. Since the percentage of silver doping the ZnO films is very low, the detection of the Zn species linked to the silver atoms is fully hidden by those Zn atoms located in the ZnO phase. Moreover, metal Zn species cannot be distinguish from Zn^{+2} cations by XPS on the basis of the main primary photoelectron signals (Zn2p), because both chemical species generates just the very same spectrum. Fortunately, the elucidation of the chemical state of Zn can be made effectively by XPS by determining the value of the modified Auger parameter[78]. For that purpose, both $Zn_{L3M45M45}$ and $Zn2p_{3/2}$ photoemission signals must be measured, since the value of the Zn modified Auger parameter, α', is equal to

the sum of the binding energy of the $Zn2p_{3/2}$ photoelectron peak and the kinetic energy of the $Zn_{L3M45M45}$ Auger line.

In order to further study this second hypothesis, one film of Zn containing a small amount of Ag, was deposited by magnetron sputtering from metallic Zn and Ag targets, and analyzed by XPS. The objective was to obtain a reference sample of Ag doped with metallic Zn, and compare its $Ag3d_{3/2}$ binding energy with the one for the case of Ag doped ZnO films.

In spite of being prepared from pure Zn and Ag targets, the film of Ag doped Zn, when examined by XPS, only showed divalent zinc at the surface, characterized by a modified Auger parameter of ~2010.0 eV, very likely as a consequence of the corrosion of this metal during its exposition to the atmosphere of the laboratory. However, and as expected, the sputtering cleaning of its surface, by bombardment with Ar^+ ions, gradually remove the altered layer, and a stationary state is reached in its composition after a treatment of 120 min, treatment long enough to remove around ~12 nm. The evolution of the surface composition of this film by the ion etching treatment is neatly noticeable by the decrease in the O/Zn atomic ratio and by the changes in the shape of $Zn_{L3M45M45}$ Auger line, where a new peak at 991.8 eV of kinetic energy, due to Zn(0), rises with the sputtering treatment. In **Fig.** 10, the spectral region for $Zn_{L3M45M45}$ signal is shown for this sample at the stationary state, where the peaks for Zn(0) and Zn(+2) are labeled and the values of the respective modified Auger parameters calculated.

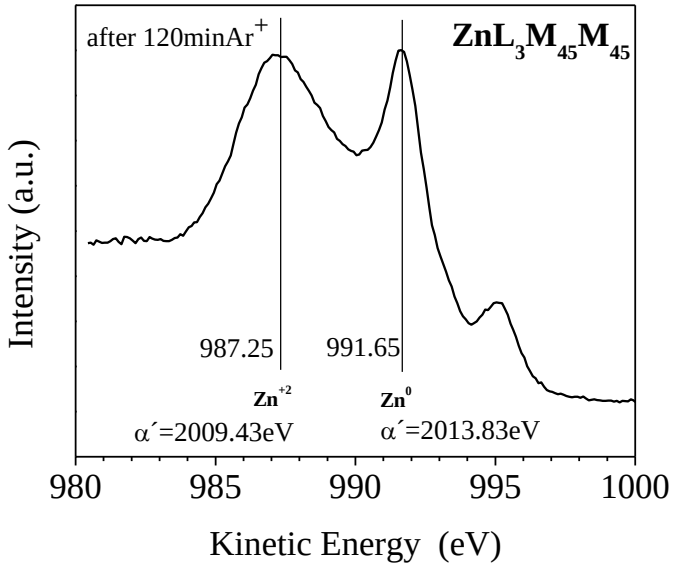

Fig. 10- Photoemission spectrum of the $Zn_{L3M45M45}$ Auger line for the Zn(Ag) sample after surface cleaning by sputtering with Ar^+ ions of 2.5 keV for 120 min.

As the morphology of this coating is highly columnar, even at the stationary state the collected XPS signal presents the contribution of the corroded lateral surface of the columns.

Fig. 11Fig. 11 shows the Zn2p and Ag3d photoemission signals of this silver doped zinc film at the original state (surface corroded) and at the stationary state after sputtering. As can be seen, $Zn2p_{3/2}$ peak appears in both situations at around 1022.20 eV of binding energy, while $Ag3d_{5/2}$ peak shifts with the sputtering treatment from 368.64 to 369.47 eV. The intensities of both Zn and Ag signals increase with this treatment, as a result of the removal of surface contaminants and, very likely, the preferential sputtering of oxygen. Obviously, the binding energy of the $Ag3d_{5/2}$ peak, 369.47 eV, is so high that it cannot be ascribed to pure metallic silver, although consisting of very small particles. Since it increases simultaneously with the detection of metallic zinc, the formation of a Zn-Ag bond is the most probable explanation for this high value of binding energy. In other words, while the presence of very small aggregates of silver

(first hypothesis) could only account for a binding energy shift of up to +0.6 eV, the doping of these particles with Zn (second hypothesis) could explain by itself the whole experimental shift and even further.

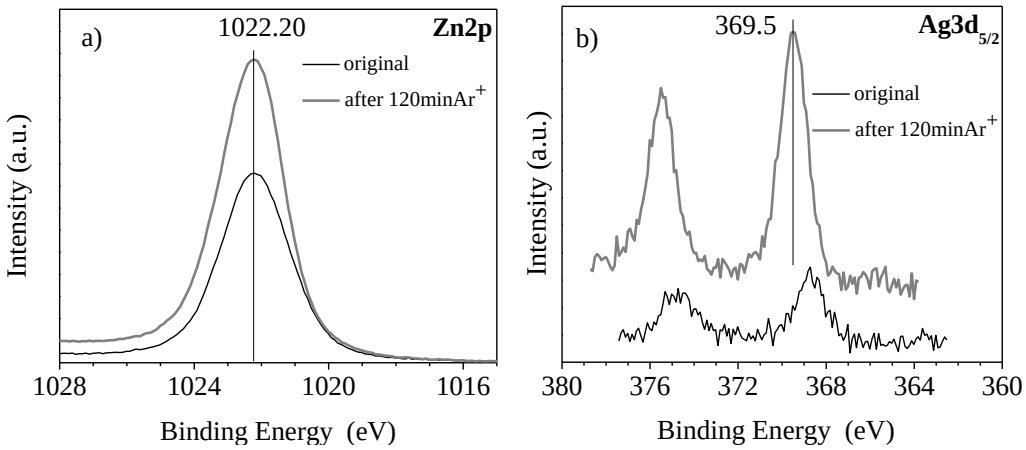

Fig. 11. XPS Zn2p (a)) and Ag3d (b)) spectra of silver doped zinc film at the original state and after 120 min of surface etching with Ar^+ ions of 2.5 keV .

Fig. 12 shows the top and cross section micrographs of the silver doped ZnO thin films.

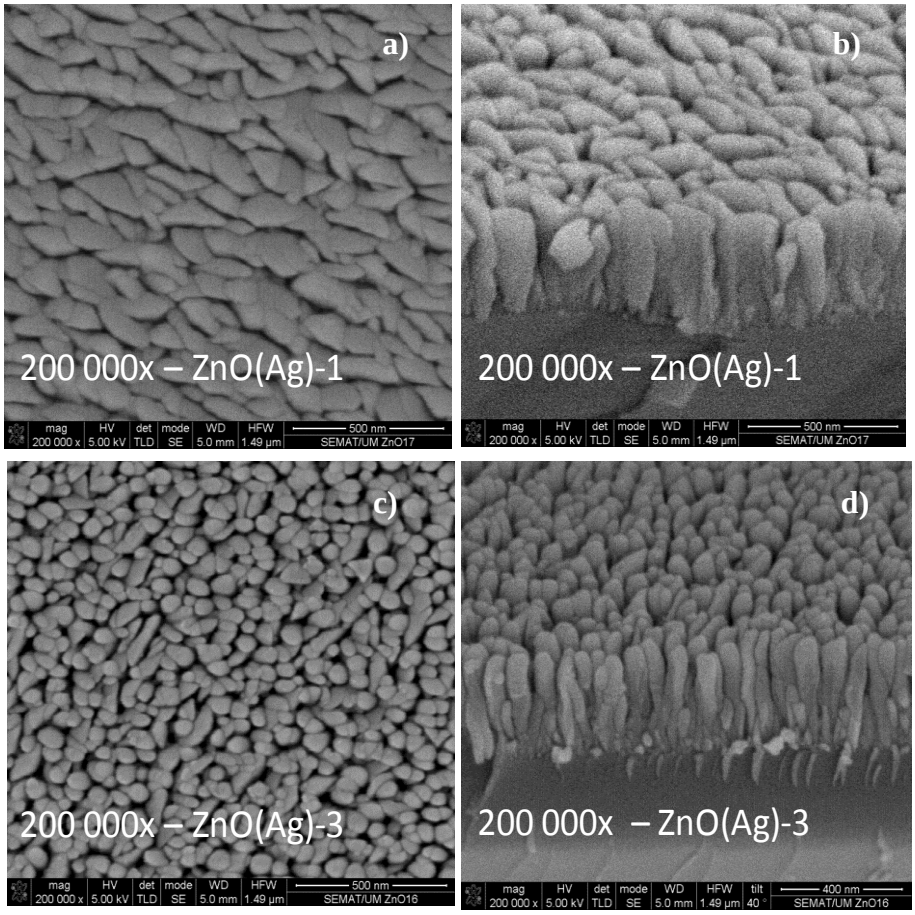

Fig. 12. Top-view and cross section SEM micrographs of silver doped ZnO thin films; a) and b) ZnO(Ag)-1 sample, c) and d) ZnO(Ag)-3 sample.

From the previous figure it is possible to observe that the presence of silver induces a change in the ZnO coatings morphology in comparison with Fig. 2b. For the samples with very low silver content, ZnO(Ag)-1 and 2 (not showed here), the shape of the columns change from circular pillar-like morphology (see **Fig. 2**) to triangular morphology (see **Fig. 12**), maintaining a V shape form in the cross section view. It is important to note that these samples do not show a crystalline preferential growth, in contrast with the undoped zinc oxide samples. The sample with the highest silver content presents a columnar morphology with a circular shape, similar to the undoped samples, but with a much less dense morphology, where the space between columns is cleared observed. Once more time, the circular columnar morphology is related to a

preferential orientation of the c-axis perpendicular to the substrate surface (see **Fig. 6**). This result suggests that the different crystalline growth related with the presence of silver could induce morphology changes in the coatings. *L.N. Wang, et al.* [79] reported that Ag doping could cause morphological changes in the ZnO thin films. The authors observed that the presence of silver induces the formation of a porous morphology.

The antibacterial activities of undoped and Ag-doped ZnO thin films against *E. coli* are depicted in Fig.7.

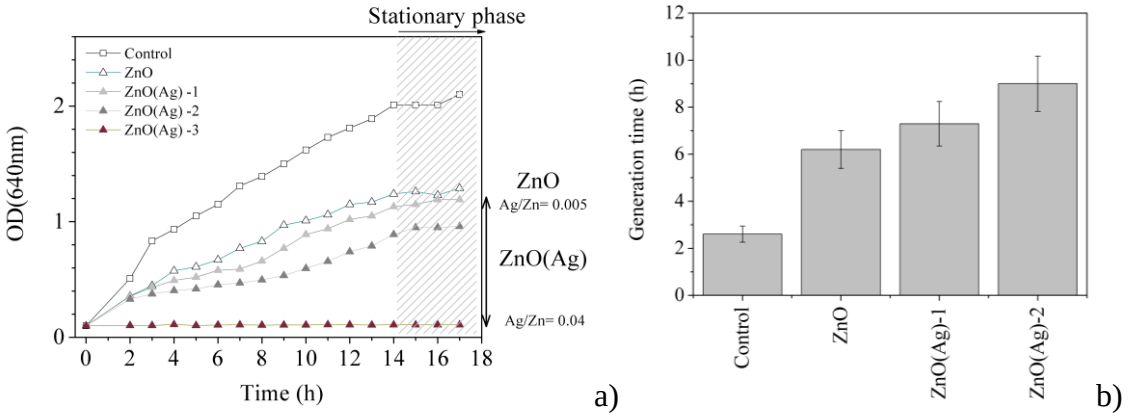

Fig. 13. Antibacterial activities of undoped and Ag- doped ZnO thin films against *E. coli*. **a)** Optical density (OD) at 640 nm over time of incubate bacteria cells with different Ag content The control growth was assessed using non coated PET with the same area; **b)** generation time of *E. coli*. bacteria.

From the previous plot (**Fig. 13**) it is possible to observe an enhancement of antibacterial activity with the increase of silver content in the zinc oxide based coatings. With the increase of silver content there is a decrease of *E. coli*. growth rate (see, **Fig. 13.a)** and 7.**b)),** a decreased amount of bacteria cells present at the end of the experiment. On the other hand for the sample having the highest Ag/Zn atomic ratio of 0.04 it is observed a complete growth inhibition (see, Fig. 13.a).

The antibacterial mechanism of ZnO is still under investigation. Two major mechanisms have been suggested: (1) the release of Zn^{2+} ions from the coating [80] and

(2) the generation of hydrogen peroxide as well as radical oxygen species from ZnO surface[81,82,83,84,85,86].

Sugarman [87] suggested that zinc ions binds to the membranes of microorganisms, extending the lag phase of the growth cycle and increasing the generation time of the microorganisms [88]. Others authors [89,90,91], observed that Zn^{2+} ions do not have much antibacterial activity up to a concentration of $7.3x10^{-5}$ M, the same order of magnitude of the solubility of ZnO in the solution. This may be consistent with the prediction that E. coli can metabolize Zn^{2+} as an oligoelement[92]. This suggests that these ions are not primarily responsible for the antibacterial activity of ZnO. The same authors claimed that the antimicrobial dominant mechanism should result from Radical Oxygen Species (ROS) generation and their subsequent interaction with cell.

Regarding the generation of highly reactive species, such as $OH^{\bullet}$ radicals, H_2O_2 and $^{\bullet}O_2^{2-}$, *Nagarajan Padmavathy and co authors*[93] explained as follows: ZnO with defects can be activated by both UV and visible light, which will induce electron-hole pairs (e^-/h^+) generation. Water molecules can spontaneously dissociate into OH^- and H_3O^+ species. Dissolved oxygen molecules are transformed to superoxide radical anions $^{\bullet}O_2^-$, that in turn will react with H_3O^+ to generate ($HO_2^{\bullet}$) radicals, which upon subsequent collision with electrons produce hydrogen peroxide anions (HO_2^-). Then, they then react with H_3O^+ to produce H_2O_2 molecules. However, light is needed to produce photocatalytic ROS. Since in the present work the *E. coli*. A- Bacteria cells were incubated in dark conditions, the generation of (ROS) cannot be explained by a photocatalytic mechanism. By another hand, *Ken Hirota et al.*[94] and *J. Sawai et al.*[95] observed the generation of •OH radicals from ZnO ceramics in dark conditions. Both authors did not explain the formation mechanism of these radicals.

Regarding the silver antimicrobial activity, silver cation (Ag^+) is highly reactive since it binds strongly to electron donor groups containing sulphur, oxygen or nitrogen[96], but metallic silver has only slight antibacterial effects because it is chemically stable[97]. Biological molecules usually contain these components in the form of thiol, amino, imidazole, carboxylate and phosphate groups. The bonding of silver ions to bacterial Deoxyribonucleic acid **(**DNA)[98] may inhibit a number of important transport processes, such as phosphate and succinate uptake and can interact with cellular oxidation processes as well as the respiratory chain[99]. It was also shown that Ag+ bonds to functional groups of proteins resulting its denaturation[100]. It is also supposed that DNA loses its replication ability and cellular proteins become inactivated on Ag^+ treatment [101]. Concerning to our specific results, some questions still remain to t be answered. They are related with the chemical activity of silver that enhances the antimicrobial effect or its influence in the coatings morphology that induces an increase of the antimicrobial effect. As shown in this work, the coatings morphology was greatly influenced the antimicrobial performance of the coatings and the presence of silver strongly changes the active surface area of the coatings. Further studies will be performed to clarify this questions.

Conclusions

ZnO thin films, with thickness varying from 50 to 600nm, were prepared by DC Reactive Magnetron Sputtering. Silver doped Zinc Oxide thin films (ZnO(Ag)) with different silver content and thicknesses closed to 200nm were also produced. All the deposited zinc oxide and silver doped ZnO coatings present a columnar morphology with V-shaped columns. The increase of coatings thickness until 200nm increases the active surface area of the columns whereas further increasing the thickness induces a

decrease of the ratio of the columns surface area and columns length. This results in a saturation of the active surface area of the thin films. All the ZnO based thin films present a hexagonal wurtzite type (JPCDS36-1451) and no additional phases of to silver or silver oxides were detected in the doped samples. The XRD results reveal that Ag^{+} should substitute Zn^{2+} ions in the zinc oxide matrix leading to a distortion of the crystalline structure. XPS analysis revealed high values of binding energy of Ag3d indicating a possible formation of a Zn-Ag bond in the zinc oxide coatings. In the case of antimicrobial properties, thin films with 50 to 100 nm present an increase of generation time by a factor of 1.26 and 1.4, respectively. By another hand the thin films with 200nm to 600nm induced an increase of the generation time by a factor from 2 to 3.3. The thickest coating (200-600nm) showed a reduction in the number of bacterial cells at the end of the experience, that was 45% at the stationary phase. This characteristic is extremely important for food packaging applications because it may reduce bacterial load. Ag-doping of ZnO enhances their antibacterial activities. In fact, with the increase of silver content there exists a decrease of *E. coli*. growth rate and a decreased of the amount of bacteria cells present at the end of the experiment (until a complete growth inhibition for the sample with a Ag/Zn atomic ratio of 0.04).

ACKNOWLEDGEMENTS

The work described in this paper is supported by project NANOPACKSAFER: NANO-engineered PACKaging systems for improving quality, SAFEty and health characteristics of foods, Portugal-Spain International Nanotechnology Laboratory

Nanotechnology Projects Call; and also by the FEDER funding through the COMPETE program and FCT PEst-C/BIA/UI4050/2011 project.

References

[1] J.D. Greig, , E.C.D. Todd, , C.A. Bartleson, , B.S. Michaels 70 (2007) J. Food Protect. 1752-1761.

[2] D. Vugia, A. Cronquist, J. Hadler, M. Tobin-D'Angelo, D. Blythe, K. Smith, , S. Lathrop, D. Morse, P. Cieslak, J. Dunn, P. L. White, J.J. Guzewich, O. L. Henao, R. M. Hoekstra, E. Scallan, , F. J. Angulo, P. M. Griffin, R. V. Tauxe, C. Barton Behravesh, Morbidity and Mortality Weekly Report. 57 (2008) 366–370.

[3] D. Davies, Nature Reviews Drug Discovery 2 (2003) 114.

[4] U. Desselberge, J. Infect 40 (2000) 3-15.

[5] R. Villalobos, P. Hernandez-Munoz, A. Chiralt , Food Hydrocolloid **20** (2006) 502-509.

[6] Ivan Sondi, Branka Salopek-Sondi, Journal of Colloid and Interface Science 275 (2004) 177–182

[7] Thawatchai Maneerung, Seiichi Tokura, Ratana Rujiravanit, Carbohydrate Polymers 72 (2008) 43–51.

[8] Qilin Cheng, Chunzhong Li, Vladimir Pavlinek, Petr Saha, Huanbing Wang, Applied Surface Science 252 (2006) 4154–4160.

[9] Osamu Yamamoto, International Journal of Inorganic Materials 3 (2001) 643–646.

[10] J. J. VORA, S. K. CHAUHAN, K.C.PARMAR, S.B.VASAVA, E-Journal of Chemistry **6(2) (**2009) 531-536

[11] Venubabu Thati, Aashis.S.Roy, M.V.N.Ambika Prasad C. T. Shivannavar, S.M.Gaddad S.M.Gaddad , J Biosci Tech, (2) (2010) 64-69.

[12]M. Heinlaan, , A. Ivask, , I. Blinova, , H. C. Dubourguier, A. Kahru, , *Chemoshere*, 71 (2008)1308-1316.

[13] V. Aruoja, , H. C. Dubourguier, , K. Kasemets, A.Kahru, *Sci. Total Environ*., 407 (2009)1461–1468.

[14] R. Wang, , J. H. Xin, , X. M. Tao, W. A. Daoud, , *Chem. Phys. Lett*., **398** (2004) 250-255.

[15] Yadav, A., Prasad, V., Kathe, A. A., Raj, S., Yadav, D., Sundaramoorthy, C., and Vigneshwaran, N., Functional Finishing in
Cotton Fabrics Using Zinc Oxide Nanoparticles, *Bull. Mater. Sci*., **29**, 641–645 (2006).

[16]S. M. Hussain, K. L. Hess, J. M. Gearhart, K. T. Geiss, J. J. Schlager, Toxic. In Vitro 19 (2005) 975.

[17] T. R. Pisanic, II, J. D.Blackwell, V. I. Shubayev, R. R. Fiñones, S. Jin, Biomaterials 28 (2007) 2572.

[18] I. Brigger, C. Dubernet, P. Couvreur, AdV. Drug DeliVery ReV. 54 (2002) 631.

[19] C.W. Lam, J.T. James, R. McCcluskey, R.L .Hunt, Toxicol Sci 77 (2004) 126–134.

[20] A. Fujishima, , T.N. Rao, D.A. Truk, J. Photochem. Photobiol. C: Photochem. Rev., 1 (2000) 1-21.

[21] Chi-Jen Chung,Hsin-I Lin, Hsi-Kai Tsou, Zhi-Yuan Shi, Ju-Liang He, Journal of Biomedical Materials Research Part B: Applied Biomaterials Volume 85B (2007) Issue 1.

[22] J. Fahlteich, M. Fahland, W. Schönberger, N. Schiller Thin Solid Films 517 (2009) 3075–3080.

[23] American Society for Testing and Material. *Powder Diffraction Files*; Joint
Committee on Powder Diffraction Standards: Swarthmore, PA, 1999, pp 3-888.

[24] Y. Yang, X.W. Sun, B.J. Chen, C.X. Xu, T.P. Chen, C.Q. Sun, B.K. Tay, Z. Sun, Thin Solid Films 510 (2006) 95 – 101.

[25] Don Klaitabtim, Sirapat Pratontep, Jiti Nukeaw, Ceramics International 34 (2008) 1103–1107

[26] J. W. Shin, J. Y. Lee, T. W. Kim, Y. S. No, W. J. Cho, W. K. Choi, Applied Physics Letters 88 (2006) 091911.

[27] N. Fujimure, T. Nishhara, S. Goto, J. Xua, and T. Ito, J. Cryst. Growth
130 (1993) 269.

[28] J. P. Zheng and H. S. Kwok, Thin Solid Films 232 (1993) 99.

[29] D. Bao, H. Gu, A. Kuang, Thin Solid Films 312 (1998) 37.

[30] S. Amirhaghi, V. Craciun, D. Craciun, J. Elder, I.W. Boyd, Microelectron. Eng. 25 (1994) 321.

[31] Eugenia Mirica, Glen Kowach, Henry Du, Crystal Growth & Design, 4 (1)(2004) 157-159.

[32] J. W. Shin, J. Y. Lee, T. W. Kim, Y. S. No, W. J. Cho, W. K. Choi, Applied Physics Letters 88 (2006) 091911.

[33] A. van der Drift, Philips Res. Rep. 22 (1967) 267.

[34] G. Knuyt, C. Quaeyhaegens, J. D'Haen, L.M. Stals, Thin Solid Films 258 (1995) 159.

[35] G. Knuyt, C. Quaeyhaegens, J. D'Haen, L.M. Stals, Phys. Status Solidi B 195 (1996) 179.

[36] Y.j. Jeon, S.K. Kim, Carbohydr Polym 41 (200) 133-141.

[37] J. Sawai, J Microbiol Methods 54 (2003) 177–182.

[38] Nicole Jones, Binata Ra, Koodali T. Ranjit, Adhar C. Manna ,FEMS Microbiol Lett 279 (2008) 71–76

[39] Lingling Zhang, Yunhong Jiang, Yulong Ding, Nikolaos Daskalakis, Lars Jeuken, Malcolm Povey, Alex J. O'Neill, David W. York, J Nanopart Res 12 (2010) 1625–1636.

[40] O. Yamamoto, Int. J. Inorg. Mater. 3 (2001) 643.

[41] Shantikumar Nair, Abhilash Sasidharan, V. V. Divya Rani, Deepthy Menon, Seema Nair, K. Manzoor, Satish Raina, J Mater Sci: Mater Med 20 (2009) 235–241.

[42] T. Jin, D. Sun, J.Y. Su, H. Zhang, H.-J. Sue, Journal of Food Science 74 (1) (2009) 47-52

[43] Shantikumar Nair, Abhilash Sasidharan, V. V. Divya Rani, Deepthy Menon, Seema Nair, K. Manzoor, Satish Raina, J Mater Sci: Mater Med 20 (2009) 235–241.

[44] O. Yamamoto, Int. J. Inorg. Mater. 3 (2001) 643–646.

[45] J.H. Li, R.Y. Honga, M.Y. Li, H.Z. Li, Y. Zheng, J. Ding, Progress in Organic Coatings 64 (2009) 504–509.

[46] L. Duan, B.X. Lin, W.Y. Zhang, S. Zhong, Z.X. Fu, Appl. Phys. Lett. 88 (2006) 232110.

[47] D.R. Sahu, Materials Science and Engineering B 171 (2010) 99–103

[48] D.R. Sahu, Microelectron. J. 38 (2007) 1252.

[49] Oleg Lupan, Lee Chow, Luis K. Ono, Beatriz Roldan Cuenya, Guangyu Chai, Hani Khallaf,† Sanghoon Park, Alfons Schulte J. Phys. Chem. *C 114, (*2010) 12401.

[50] Y.Chen, X.L.Xu, G.H.Zhang, H.Xue, S.Y.Ma, Physica B 404 (2009) 3645–3649

[51] Y.F. Yang, M.M. Al-Jassim, S.H. Wei, Appl. Phys. Lett. 89 (2006) 181912.

[52] Y. Zhang, Z.Y. Zhang, B.X. Lin, Z.X. Fu, J. Phys. Chem. B 109 (2005) 19200.

[53] S.H. Jeong, B.N. Park, S.B. Lee, J.H. Boo, Surf. Coat. Technol. 193 (2005) 340.

[54] E. Rita, U. Wahl, A. M. L. Lopes ,J. P. Araújo, J. G. Correia, E. Alves, J. C. Soares, Physica B 340(2003)240.

[55] Shu-Ting Kuo, Wei-Hsing Tuan, Jay Shieh, Sea-Fue Wang, Journal of the European Ceramic Society 27 (2007) 4521–4527

[56] Y. Yan, M. M. Al-Jassim, S. Wei, Appl. Phys. Lett. 89 (2006) 181912.

[57] Q. Wan, Z. Xiong, J. Dai, J. Rao, F. Jiang, Opt. Mater. **30** (2008).817

[58] Shu-Ting Kuo, Wei-Hsing Tuan, Jay Shieh, Sea-Fue Wang, Journal of the European Ceramic Society 27 (2007) 4521–4527

[59] Shu-Ting Kuo, Wei-Hsing Tuan, Jay Shieh, Sea-Fue Wang, Journal of the European Ceramic Society 27 (2007) 4521–4527

[60] M.N. Islam, T.B. Ghosh, K.L. Chopra, H.N. Acharya, Thin Solid Films 280 (1996) 20.

[61] A.I. Boronin, S.V. Koscheev, G.M. Zhidomirov, Journal of Electron Spectroscopy and Related Phenomena 96 (1998) 43–51

[62] J.F. Weaver, G.B. Hoflund J Phys Chem 98 (1994) 8519.

[63] S.W. Gaarenstroom, N. Winograd, J Chem Phys 67 (1977) 3500.

[64] L.H. Tjeng, M.B.J. Meinders, J. van Elp, J. Ghijsen, G.A. Sawatzky, Phys Rev B 41 (1990) 3190.

[65] J.F. Moulder, W.F. Stickle, P.E. Sobol, K.D. Bomben, Handbook of X-ray Photoelectron Spectroscopy. Eden Prairie: Parkin-Elmer; 1992. p. 172.

[66] Y. Chiu, U. Rambabu, M.-H. Hsu, H.-P.D. Shieh, C.-Y. Chen, H.-H. Lin, J. Appl. Phys. 94 (2003) 1996.

[67] W.A. Parkhurst, S. Dallek, B.F. Larrick, J. Electrochem. Soc. 131 (1984) 1739.

[68] S. Dallek, W.A. West, B.F. Larrick, J. Electrochem. Soc. 133 (1986) 2451.

[69] M.G.Mason, Physical Review B, 27(2) (1983) 748-762.

[70] M.G.Mason, Physical Review B, 27(2) (1983) 748-762.

[71] J.A.Rodríguez, M.Kuhn and J.Hrbek. J.Phys.Chem. 100 (1996) 18240-18248.

[72] K.Lou, T.P.St.Clair, X.Lai and D.W.Goodman. J.Phys.Chem. B, 104 (2000) 3050-3057.

[73] K.Lou, T.P.St.Clair, X.Lai and D.W.Goodman. J.Phys.Chem. B, 104 (2000) 3050-3057.

[74] M.G.Mason, Physical Review B, 27(2) (1983) 748-762.

[75] P.S.Bagus, C.R.Brundle, G.Pacchioni, F.Parmegiani, Surf. Sci. Rep. 19 (1993) 265.

[76] G.K. Wertheim, S.B.DiCenzo, D.N.E.Buchanan, Physical Review B 33 (1986,)5384

[77] W.F.Jr. Egelhoff, G.G.Tibbetts, Physical Review B, 19 (1979) 5028.

[78] C.D.Wagner, Faraday Discuss. Chemical Soc., 60 (1975) 291.

[79] L. N. Wang, L.Z.Hu, H.Q.Zhang, Y.Qiu,Y.Lang, G.Q.Liu,J.Y.Ji, J.X.Ma,Z.W.Zhao, Materials Science in Semiconductor Processing 14 (3-4) (2011) 274.

[80] M. Heinlaan, A. Ivask, I. Blinova, H.C. Dubourguier, A. Kahru, Chemosphere 71 (2008) 1308–16.

[81] S.J. Chen, Y.C. Liu, C.L. Shao, R. Mu, Y.M. Lu, J.Y. Zhang, Adv Mater 17 (2005) 586-90.

[82] J. Sawai, S. Shoji, H. Igarashi, A. Hashimoto, T. Kokugan, M. Shimizu, J Ferment Bioeng 86 (1998) 521–2.

[83]J. Sawai, S. Shoji, H. Igarashi, A. Hashimoto, T. Kokugan, M. Shimizu, H. Kojima, Ferment. Bioeng. 86 (1998) 521–522.

[84] R. Brayner, R. Ferrari-Iliou, N. Brivois, S. Djediat, M.F. Benedetti, F. Fievet, Nano Lett 6 (2006) 866–70.

[85] T. Xu, CS. Xie, Prog Org Coat 46 (2003) 297–301.

[86] J. Sawai, S. Shoji, H. Igarashi, A. Hashimoto, T. Kokugan, M. Shimizu, H. Kojima, J. Ferment. Bioeng. 86 (1998) 521–522.

[87] B. Sugarman, Rev. Infect. (1983) 138-147.

[88] L.L. Radke, B.L. Hahn, D.K. Wagner, P.G. Sohnle, Clinical Immun. And Immuno. Pathol. 73(3) (1994) 344-349.

[89] J. Sawai, Journal of Microbiological Methods 54 (2003) 177– 182.

[90] Lingling Zhang, Yunhong Jiang, Yulong Ding, Nikolaos Daskalakis, Lars Jeuken, Malcolm Povey, Alex J. O'Neill, David W. York, J Nanopart Res 12 (2010) 1625–1636.

[91] Guy Applerot, Anat Lipovsky, Rachel Dror, Nina Perkas, Yeshayahu Nitzan, Rachel Lubart, Aharon Gedanken, Adv. Funct. Mater. 19 (2009) 842–852.

[92] M. Roselli, A. Finamore, I. Garaguso, M.S. Britti, E. Mengheri J. Nutr. 133 (2003) 4077-4082.

[93] Nagarajan Padmavathy, Rajagopalan Vijayaraghavan, Sci. Technol. Adv. Mater. 9 (2008) 035004.

[94] Ken Hirota, Maiko Sugimoto, Masaki Kato, Kazuhiko Tsukagoshi, Tooru Tanigawa, Hiroshi Sugimoto, Ceramics International 36 (2010) 497–506.

[95] J. Sawai, E.Kawada, F.Kanou, H. Igarashi., A. Hashimoto, , T. Kbkugan, , M. Shimizu, J. Chem. Eng. Japan, 29 (1996) 627-633.

[96] J. M. Schierholz, L. J. Lucas, A. Rump, G. Pulverer, journal of Hospital Infection 40 (I 998) 257-262.

[97] J. M. Schierholz, L. J. Lucasj, A. Rump, G. Pulverer, journal of Hospital Infection 40 (I 998): 257.

[98] K. Modak, C. Fox, Biochem Pharm 22 (1973) 2392-2404.

[99] J. M. Schierholz, L. J. Lucas, A. Rump, G. Pulverer, journal of Hospital Infection 40 (I 998) 257-262.

[100] J.A. Spadaro, T.J. Berger, S.D. Barranco, S.E. Chapin, R.O. Becker, Microb. Agents Chemother. 6 (1974) 637.

[101] Q.L. Feng, J. Wu, G.Q. Chen, F.Z. Cui, T.M. Kim, J.O. Kim, J. Biomed. Mater. Res. 52 (2000) 662.